Application of a Comprehensive Lagrangian-Eulerian Spark-Ignition Model to Different Operating Conditions

Samuel J. Kazmouz[1], Riccardo Scarcelli[1], Matthew Bresler[2]
[1] Argonne National Laboratory, Lemont, IL 60439, [2]FCA US LLC, Auburn Hills, MI 48326

Abstract

Increasing engine efficiency is essential to reducing emissions, which is a priority for automakers. Unconventional modes like boosted and highly dilute operation have the potential to increase engine efficiency but suffer from stability concerns and cyclic variability. To aid engineers in designing ignition systems that reduce cyclic variability in such engine operation modes, reliable and accurate spark ignition models are necessary. In this paper, a Lagrangian-Eulerian spark ignition (LESI) model is used to simulate electrical discharge, spark channel elongation, and ignition in inert or reacting crossflow within a combustion vessel, at different pressures, flow speeds, and dilution rates. First the model formulation is briefly revisited. Then, the experimental and simulations setups are presented. The results showcase the model's ability to predict the secondary circuit voltage, current, and power signals, in addition to the spark channel elongation, for the inert cases, or flame front growth, for the reacting cases. The results also compare simulation spark channel and flame growth plots to experimental Schlieren images at different instants in time. This work serves to highlight LESI's ability to predict the characteristics of discharge and ignition across a variety of operating conditions.

Introduction

The transportation sector in the United States is responsible for the largest share of energy consumption and CO_2 emissions [1]. Light duty vehicles (LDV), which are the most common form of transportation, generally rely on four-stroke gasoline spark-ignition (SI) internal combustion engines (ICEs). ICEs have become popular due to low production costs, low maintenance costs, and large availability of gasoline distribution infrastructure. While electrification of LDVs by original equipment manufacturers (OEMs) and recent government-driven policy changes predict an uncertain future, SI engines will remain a large part of the market by 2050 [1]. In addition, spark ignition systems will still be relevant in several applications including gasoline electric hybrid vehicles, heavy duty vehicles, and off-road engine applications.

Emissions reduction through efficiency improvements of ICEs is a plausible path that automakers are pursuing. Highly dilute, stratified-charge, and boosted operation modes promise an increase in SI-engine efficiency [2]. The engine is characterized by high levels of dilution or overall lean operation, which improve efficiency by reducing heat loss and improving knock tolerance [3]. In these modes the engine runs more efficiently but experiences instability and elevated levels of cyclic variability which originate from the early stages of combustion with flame-to-spark plug contact area variation [4], turbulent flame growth fluctuations [5], flame kernel displacement [6], dependence on flame speed, especially at lean limits [7], and injection-turbulence interaction and variability [8]. As a result, ignition systems must provide more energy for a longer duration compared to traditional engine operation to ensure stable combustion [9]. Hence, predictive spark ignition models are necessary to design ignition systems that reduce cyclic variability in these operation modes.

Eulerian ignition models [10, 11, 12] initialize ignition criteria such as energy, temperature, fuel mass fraction, or flame surface density on a finite volume grid and allow the pressure and temperature to expand [13]. A spherical energy deposition approach is commonly used by industry, but cylinder and line shapes are also utilized [14, 15]. As smaller grid sizes became feasible with increased computational power, Eulerian grids were used to simulate complex engine geometries with multiple ignition sources [16]. Furthermore, the ignition sources became of complex shapes that can be held stationary or allowed to move with the flow. Two common Eulerian ignition models are GLIM [17] which targets dilute operating conditions, and ISSIM [12] which couples with the coherent flame model (CFM) through a flame surface density transport equation and transition function.

On the other hand, Lagrangian models [18, 19, 20] treat the spark channel as a series of points that are tracked in time and space. Then, at the location of the points, flame kernels are initialized and their size tracked using physics-based combustion and transport correlations. It is only after the flame kernel reaches a critical size that a turbulent flame propagation model takes over. In fact, many Lagrangian ignition models were developed to be coupled with specific combustion model [12, 20]. DPIK [21], AKTIM [19], and SparkCIMM [20] are among the most common Lagrangian models. In these models the spark channel is tracked using flame speed expressions and a flame kernel initialized using specific criteria, such as Karlovitz number. Furthermore, some Lagrangian ignition models rely on stochastic perturbation elements to modify the particle velocities and incorporate cyclic variability [22, 23]. Such approaches aim at improving the modeling of ignition systems and their effect on the cyclic variability of combustion under lean conditions.

Despite the distinction between the two approaches, ignition models do not have to fall exclusively under one category. In fact, recent ignition models including the one to be presented here, comprise of both Lagrangian and Eulerian formulations [24, 25]. The spark channel elongation is tracked with Lagrangian points and high-

fidelity energy deposition is achieved through a fine computational grid.

In addition to the spark channel elongation capabilities, modern ignition models require additional sub-models to handle spark channel shortening events. During high turbulence conditions, the spark channel elongates downstream and can stretch, twist, and possibly trigger short-circuit or restrike events [26, 27, 28]. Early research did not draw a distinction between short-circuit and restrike events and both were triggered when the potential difference (or voltage) exceeded a threshold value [29, 30]. Later research distinguished between short-circuits as voltage-dependent events and blowout/restrikes as current-dependent events. Short-circuits occur when the voltage between two internal Lagrangian points overcomes a calculated threshold followed by a subsequent discharge occurring between the two points and the excess spark channel dissipating. On the other hand, a blowout occurs when overall system current drops below a calculated threshold and the spark channel cannot be sustained. A restrike then occurs if the system (or coil) has sufficient residual energy to overcome the breakdown energy and reinstate the spark channel [31, 32, 33].

From a modeling perspective, instantaneous electrical metrics such as current and voltage are required to model spark channel shortening. This necessitates modeling the electrical system through an online secondary circuit sub-model, which is anchored around an empirical expression of the spark channel voltage [34, 35], as shown in Eq. 1:

$$R_{spk} = A\, p^{a_1}\, l_{spk}\, i^{a_2} \quad (1)$$

where p is pressure, l_{spk} is the spark channel length, and i is the current. A, a_1, and a_2 are model parameters. A has been reported in literature as 40.46 [31, 34] and 60 [33], a_1 is reported to be 0.51 [31, 33, 34], and a_2 is reported to be -1.32 [31, 34] and -1.1 [33].

Implementation of spark shortening sub-models in literature generally relies on involved ignition criteria that are often validated in one flow or combustion operating conditions. In this paper, the Lagrangian-Eulerian Spark-Ignition (LESI) model developed in earlier work [36, 37, 38] is utilized to model electrical discharge, ignition behavior, and spark channel elongation and shortening, in different flow and combustion operating conditions. LESI provides a predictive framework to track spark channel elongation and secondary circuit electric waveforms during discharge or ignition. It couples seamlessly with common combustion and turbulence models in a computational fluid dynamics (CFD) framework and will be discussed in detail in the next section. LESI's formulation makes used of the Eulerian flow and combustion solution variables to leverage fine grids and increase the accuracy of spark channel elongation and ignition modeling.

The paper is structured as follows. First, the model development is revisited and summarized in the methods section. Then, the simulation and experimental setups are presented. In the results section, the inert electrical discharge simulations are presented followed by reacting ignition simulations. The results are compared to experimental electrical data and Schlieren images. Finally, the model's ability to predict spark channel elongation and shortening events are highlighted through a compilation of the results.

Methods

LESI Model

At Argonne National Laboratory, prior to the development of the LESI model, ignition research began with a detailed energy deposition study in a quiescent condition which concluded accurate source geometry, heat transfer, and detailed chemistry are necessary to predict ignition success and misfire conditions. [39].

Building on the previous findings, LESI combined Lagrangian and Eulerian approaches to model spark channel elongation during the glow-phase of ignition in non-quiescent conditions. LESI was built within the CONVERGE CFD framework through user defined functions (UDFs) [40]. The breakdown phase of ignition can be modeled through stationary energy deposition or offline equilibrium calculations to resolve pressure, temperature, and species profiles. The main features of the model include:

1. Lagrangian approach for spark channel tracking, as a line source:
    - Spark channel elongation is not free but relies on a velocity derived from the local flow to account for spark channel impedance
    - The Lagrangian point velocity is smoothed based on neighboring points' velocities to maintain a consistent channel geometry and resist flow fluctuations that result from energy deposition
2. Eulerian approach energy deposition:
    - The energy is deposited in computation cells where the Lagrangian points exists based on a fractional distribution algorithm that relies on segment length.
3. The end points of the channel are always attached to the electrode surfaces and are allowed to move along them.
4. If a central point moves too close to an electrode surface, it becomes the new end point and the remaining spark channel length is truncated.

More recently, the LESI model was further developed to include spark channel shortening capabilities [36]. As discussed briefly in the introduction, spark shortening capabilities require electrical metrics that necessitate an online secondary circuit sub-model. The secondary circuit sub-model calculates the voltage, current, resistance, and ohmic losses of the system. It receives the total circuit energy as an input, which can be the secondary circuit energy directly or the primary circuit energy corrected with a conversion efficiency factor. The model deducts the breakdown energy (using a capacitive expression) and assumes a purely inductive discharge of the remaining glow phase energy. As time progresses, the secondary circuit sub-model goes through the following steps at every time step:

1. Calculates the electrical current from the remaining system energy and inductance
2. Calculates the spark channel voltage from the empirical resistance expression (Eq. 1), which was tuned for the dataset used
3. Calculates the deposition energy from the current, voltage, and time step values
4. Calculates the ohmic loss energy
5. Deducts the deposition and ohmic loss energy from the total system energy and transfers the deducted energy to the deposition sub-model

Following the secondary circuit sub-model, the blowout and restrike sub-model is called. First, the system's electrical current is compared to a threshold current shown in Eq. 2:

$$i_{th} = B \ {l_{spk}}^{b_1} \quad (2)$$

where i_{th} is the threshold current, then B and b_1 are model parameters. Since this sub-model is called at every timestep, a blowout is triggered when the systems electrical current drops below the threshold current. The remaining system energy is compared to the energy required to initiate another spark, i.e., breakdown energy. If the system does not have enough energy to initiate a breakdown event, that means this is the end of the discharge. If the remaining energy is sufficient, then a restrike is triggered and the spark channel is reinitialized between the electrodes.

If neither a blowout nor a restrike is triggered, then the LESI model calls the short-circuit sub-model, which scans the entire spark channel for a combination of points that meet its criteria. Two voltage values are calculated for every point combination in the spark channel. The first value is a voltage difference between two hypothetical points 1 and 2 as shown in Eq. 3:

$$V_{12} = V_{spk} \frac{l_{12}}{l_{spk}} \quad (3)$$

where V_{12} is the voltage difference between points 1 and 2, V_{spk} is the spark channel voltage, and l_{12} is the segment length between points 1 and 2 along the spark channel. The second value is a threshold voltage unique to the hypothetical point combination 1 and 2 as shown in Eq. 4:

$$V_{th} = D \ \delta l^{d_1} \ i^{d_2} \quad (4)$$

where V_{th} is the threshold voltage, δl is the direct distance in space between points 1 and 2, and $D, d_1,$ and d_2 are model parameters. The model then triggers a short-circuit between the point combination with the highest positive potential difference between the two voltage values.

Experimental Setup

The validation carried out in this work leveraged an experimental dataset provided by FCA US LLC and created at the Michigan Technological University (MTU) Advanced Power Systems (APS) Laboratory. The experiments were performed in a 1.1 L constant volume combustion vessel equipped with a shrouded fan that directs airflow towards the spark plug location and can maintain constant flow despite pressure fluctuations within the vessel. The vessel is capable of temperatures up to 2100K and pressures upwards of 340 bar. For this experimental data set, the fan was operated at 5000 and 10000 rpm at pressures of 15, 30, and 45 bar providing six operating conditions. In addition, for every condition three experiments were carried out:

1. Crossflow without ignition
2. Electrical discharge in inert crossflow
3. Ignition in dilute reacting crossflow

The spark channel, if present, was visualized using a Schlieren technique. The secondary circuit voltage and current were measured and used to calculate the discharge energy. The ambient temperature was fixed at 423 K for all experiments. The flow experiments and some of the inert electrical discharge operating conditions were used in previous validation work and will be omitted here [15, 34]. Hence, all experimental cases relevant to this work are listed in Table 1.

Table 1: Experimental operating conditions used for validation. The reported discharge energy is calculated from the experimental voltage and current signals.

Case	Type	P (bar)	Fan speed (rpm)	Discharge Energy (mJ)	Fuel/Ø/EGR%
1	Inert	15	5000	92	-
2	Inert	15	10000	94.7	-
3	Inert	30	10000	93.8	-
4	Reacting	15	5000	50	C_2H_6/1.0/20%
5	Reacting	15	10000	48.2	C_2H_6/1.0/20%
6	Reacting	30	5000	71	C_2H_6/1.0/40%
7	Reacting	30	10000	82	C_2H_6/1.0/40%
8	Reacting	45	5000	62	C_2H_6/1.0/40%
9	Reacting	45	10000	56.6	C_2H_6/1.0/40%

Simulation Setup

The RANS simulations were carried out using CONVERGE CFD solver v3.0 [40] and LESI ignition model implemented through UDFs. The computational domain of the combustion vessel is shown in Fig. 1.

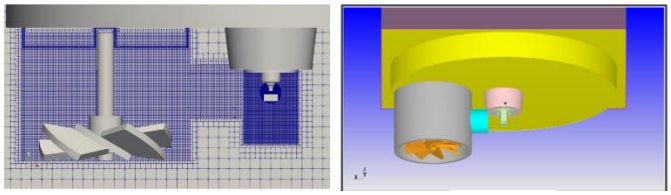

Figure 1: Computational domain and grid of the combustion vessel used in the simulations.

The impeller and its shaft are set as rotating wall boundaries, while the outer vessel wall is set as a fixed. The rest of the surfaces including the fan shroud and spark plug are set as fluid/solid interface since conjugate heat transfer modeling is active. The slab on the roof of the chamber is modeled as a solid region with the properties of stainless steel.

CONVERGE CFD creates the computation grid through its proprietary automated mesh generation method that relies on a modified cut-cell Cartesian method. The orthogonal Eulerian grid has a base size of 2 mm. Multiple fixed embedding regions are applied to the domain including the fan and its outlet, and the spark plug electrodes area. The fan region has a grid size of 250 µm while the region around the spark plug has a grid size of 125 µm and 62.5 µm near the electrodes and spark gap. In addition, adaptive mesh refinement (AMR) is active in the high temperature regions.

Electrical discharge is divided between two energy sources. The first source is stationary and represents the breakdown phase of ignition. The second source represents the glow phase as a line source of

Lagrangian points, is handled by the LESI model, and starts after the first source ends. All the simulations use a RANS standard $k-\varepsilon$ turbulence model. Time-stepping is controlled by a dynamic scheme limited by set velocity, viscosity, and sonic CFL numbers.

Combustion is modeled using the well-stirred reactor (WSR) model relying on the GRI-Mech v3.0 mechanism. While the LESI model can be coupled with the g-equation model and the thickened flame model (TFM), here the WSR is used because the grid is fine enough to provide accurate results with a detailed chemistry approach. Furthermore, ignition and flame growth predictions are validated against experimental Schlieren images. For inert cases, no mechanism was used but instead the main air species (N_2 and O_2) are tracked.

Results

The results from simulations of Cases 1-9 are shown here. For every case, the results include secondary circuit electrical current, voltage, power, and either spark channel length if inert, or flame front location if reacting. In addition, for every case the results include comparisons of the spark channel elongation with experimental Schlieren images at selected instants in time. For every section, the results conclude with a summary table of the model's prediction of spark channel shortening events as compared to experiment.

Inert Electrical Discharge Simulations: Cases 1-3

Cases 1, 2 and 3 simulate electrical discharge in an inert environment. No combustion is triggered as the ambient environment consisted of nitrogen gas.

Case 1

The ambient pressure in Case 1 is 15 bar and the fan speed is set to 5000 rpm. The fan creates a velocity field from left to right (refer to Fig. 1), stretching the spark channel in the same direction. The LESI model tracks the elongation and shortening of the spark channel. The secondary circuit output from the simulation of Case 1 is shown in Fig. 2 (a), (b), and (c), compared to two experimental iterations of the same operating condition. Fig. 2 (d) shows the spark channel length as predicted by LESI model, also compared to experiment.

In Fig. 2 (a), the inductive phase electrical current starts at around 100 mA and decreases steadily until end of discharge around 2.4 ms. On the other hand, the spark channel voltage in the inductive phase shown in Fig. 2 (b) increases with time, as the spark channel elongates. A sudden drop in voltage is observed at around 1.5 ms, which mirrors a restrike event shown in Fig. 2 (d). The spark channel length decreases from 3.5 mm to 0.6 mm (the original length at the electrode gap) and continues to grow once again as time progresses, signifying a restrike. Another sudden drop is observed at around 2.4 ms, signifying the end of discharge. The instantaneous power is shown in Fig. 2 (c), decreases slowly as time progresses, driven mainly by a decreasing electrical current.

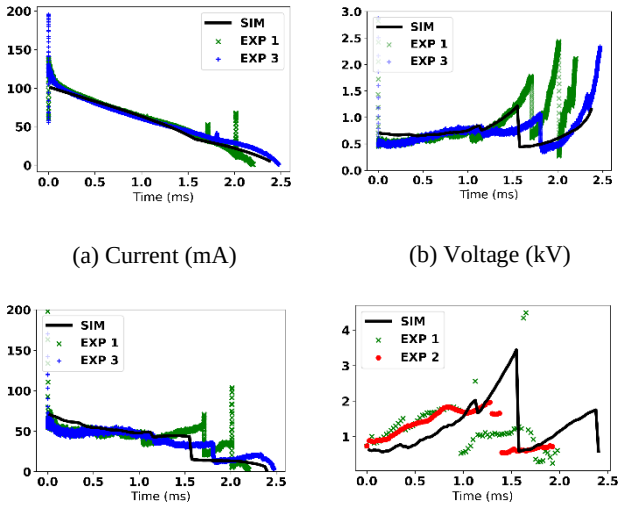

(a) Current (mA) (b) Voltage (kV)

(c) Power (W) (d) Spark Length (mm)

Figure 2: LESI model output for Case 1. The experiment numbers are different experimental iterations of the same operating condition.

All the model metrics shown in Fig. 2 agree with experimental results. The model predicts a restrike at around 1.6 ms, while the first and second experimental iterations predict a restrike at around 1.0 ms and 1.4 ms respectively.

The spatial elongation and shortening predicted by LESI model are assessed by comparisons with experimental Schlieren images. For Case 1, the results are shown in Fig. 3. The viewing window is identical and the thick white line in the simulation results is the spark channel meant to mirror the white luminous spark channel seen in the Schlieren images. The spark initialization in the experiments is a stochastic process that depends on local metrics such as spark gap, electrode geometry and edge conditions, gas composition, temperature, and pressure. Given that LESI is a glow phase model, the breakdown phase initialization is fixed as a vertical channel in the spark gap, which introduces errors at early times of discharge. However, these errors are not carried over significantly during later times of discharge.

From Fig. 3, it can be inferred that while the elongation of the central Lagrangian point matches experiment, the simulation struggles to maintain an overall arc shape and end point location that matches experiment at early times. In addition, at around 1.4 ms, a blowout and restrike are predicted by the simulation which are only seen in the experiment at around 1.9 ms. Nevertheless, the simulation correctly predicts the occurrence of a blowout and restrike, even though at an earlier time than observed. The discrepancy could be due to multiple reasons, such as flow-related inaccuracies. However, the most likely root cause is the breakdown phase. In the simulation, breakdown is initialized as a vertical channel while throughout experimental observations, that is rarely the case. The spark channel immediately after the end of breakdown has an irregular "folded" shape, which cannot be replicated in simulation without introducing a stochastic or random element.

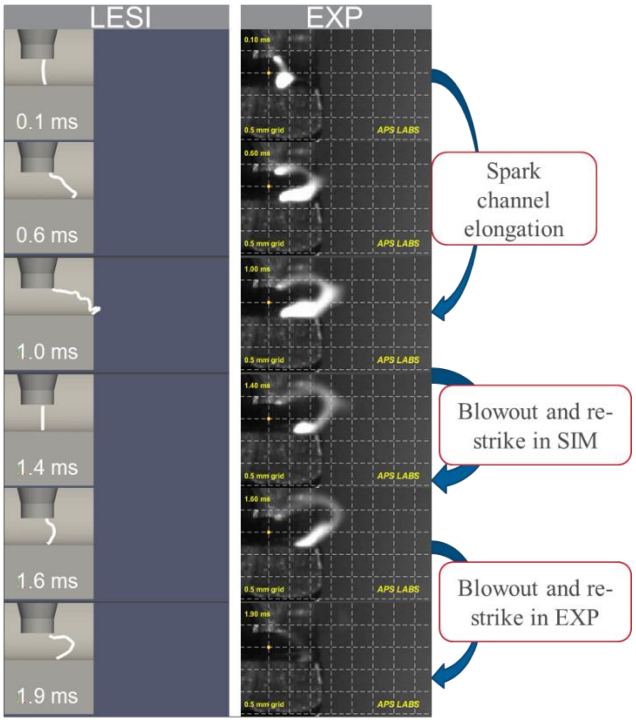

Figure 3: Spark channel elongation: simulation versus experiment Schlieren images for Case 1. Prediction of a blowout and re-strike around 1.4 ms for the simulation.

Case 2

The ambient pressure in Case 2 is 15 bar and the fan speed is set to 10000 rpm. Similar to Fig. 2, Fig. 4 shows the electrical current, voltage, power, and spark channel length compared to experiments. The inductive electrical current in Fig. 4 (a) starts at 100 mA and decreases steadily until the end of discharge at around 2.0 ms. The inductive phase voltage in Fig. 4 (b) increases until a first sudden drop at around 1.3 ms followed by another sudden drop at around 1.8 ms, both corresponding to restrikes seen in Fig. 4 (d). In addition, one short circuit is observed at around 0.7 ms in Fig. 4(d). As expected, the electrical power decreases with time as the secondary circuit energy is depleted until the end of discharge. All the model metrics shown in Fig. 4 show good agreement with experimental discharge duration and rate in addition to the occurrence of spark shortening events.

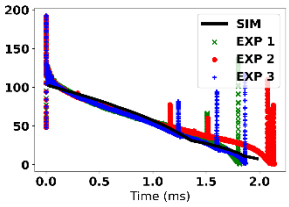

(a) Current (mA)

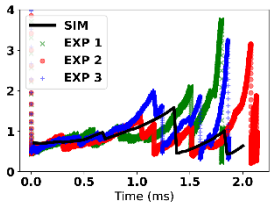

(b) Voltage (kV)

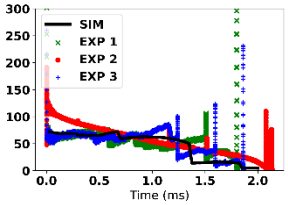

(c) Power (W)

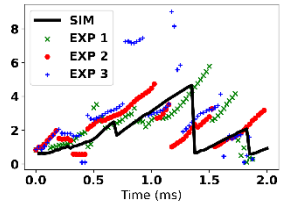

(d) Spark Length (mm)

Figure 4: LESI model output for Case 2. The experiment numbers are different experimental iterations of the same operating condition.

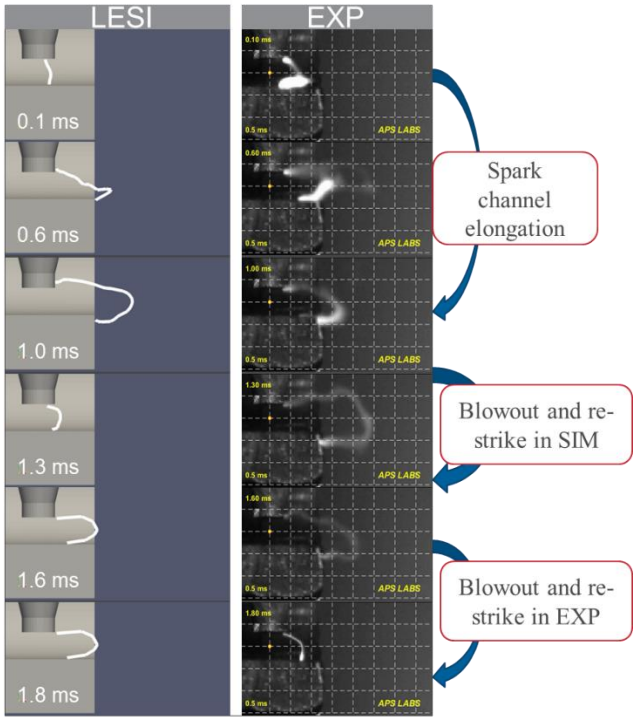

Figure 5: Spark channel elongation: simulation versus experiment Schlieren images for Case 2. Prediction of a blowout and re-strike around 1.3 ms for the simulation.

The spark channel elongation for Case 2 is shown in Fig. 5. The model exhibits good qualitative agreement in terms of arc shape and spark channel elongation for the early discharge duration (times earlier than 1.0-1.3 ms). The model predicts a blowout and restrike around 1.3 ms which are only seen in the experiment at around 1.8 ms. Nevertheless, the simulation correctly predicts the occurrence of a blowout and restrike, while maintaining good agreement in arc shape and elongation, even though it is at an earlier time. Unlike the previous case, the spark channel shape is well predicted here and errors introduced during the initialization process are not evident past t = 0.6 m.

Case 3

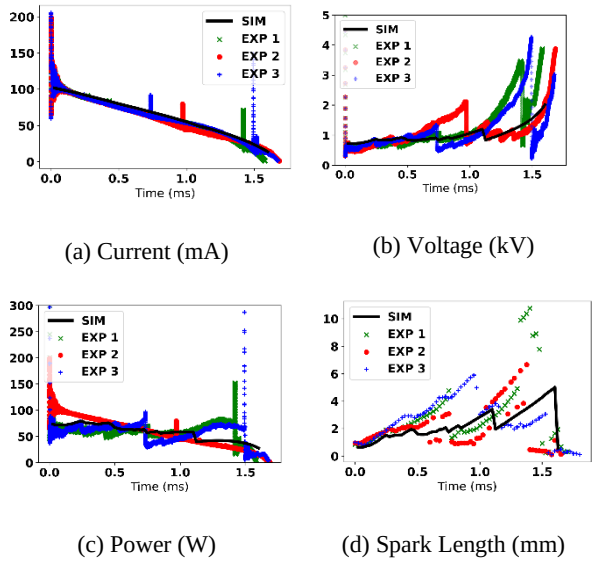

(a) Current (mA) (b) Voltage (kV)

(c) Power (W) (d) Spark Length (mm)

Figure 6: LESI model output for Case 3. The experiment numbers are different experimental iterations of the same operating condition.

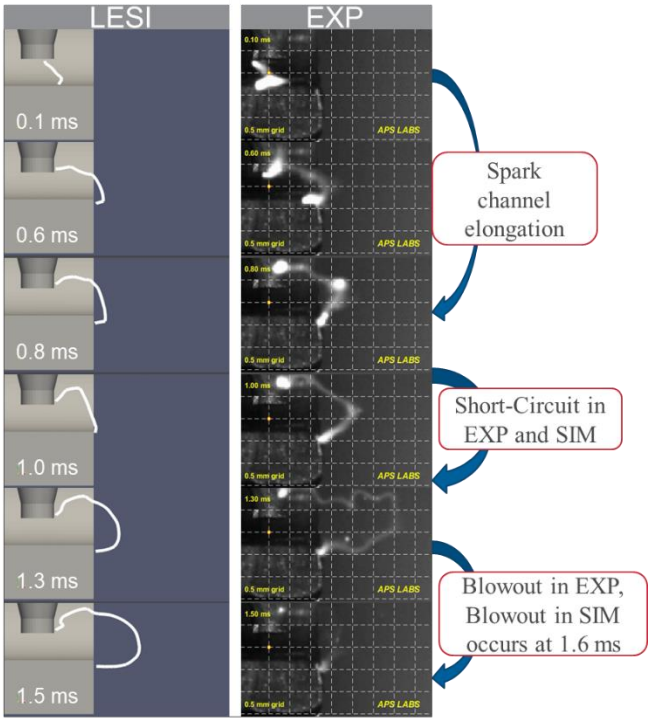

Figure 7: Spark channel elongation: simulation versus experiment Schlieren images for Case 3. Correct prediction of a short-circuit between 0.8 and 1.0 ms is shown. Blowout observed around 1.5 ms, while model predicts a blowout around 1.6 ms.

The ambient pressure in Case 3 is 30 bar and the fan speed is set to 10000 rpm. Similar to Figs. 2 and 4, Fig. 6 shows the electrical current, voltage, power, and spark channel length compared to experiments. The inductive phase electrical current in Fig. 6 (a) also starts at 100 mA and decreases steadily until the end of discharge at around 1.7 ms. The inductive phase voltage in Fig. 6 (b) increases until a sudden drop at around 1.2 ms corresponding to a short-circuit seen in Fig. 6 (d). As expected, the electrical power decreases until the end of discharge. All the model metrics shown in Fig. 6 show good agreement with experimental results.

The spark channel elongation for Case 3 is shown in Fig. 7. The simulation predicts correct movement of the end points as well as overall spark channel elongation and shape while retaining the angularity observed in the experimental images. The simulation predicts a short circuit between 0.8 and 1.0 ms, which matches the experiment. Finally, end of discharge is predicted at around 1.5 ms, which matches experimental observation of 1.6 ms. Similar to Case 2, the spark channel shape is well predicted. The shape of the arc at t = 0.1 ms matches the experiment thus eliminating initialization errors early on in the simulation and leading to excellent prediction of arc shape and growth.

Table 2: Short-circuit, blowout, re-strike, and end of discharge time of occurrence predictions made by the LESI model, compared to experiment for cases 1-3

Case	Short Circuit (ms)	Blowout (ms)	Restrike (ms)	End of Discharge (ms)
1 – SIM	-	1.4	1.4	2.4
1 – EXP	-	1.9	1.9	2.5
2 – SIM	-	1.3	1.3	2.0
2 – EXP	-	1.8	1.8	1.9
3 – SIM	1.0	1.6	-	1.7
3 – EXP	1.0	1.5	-	1.7

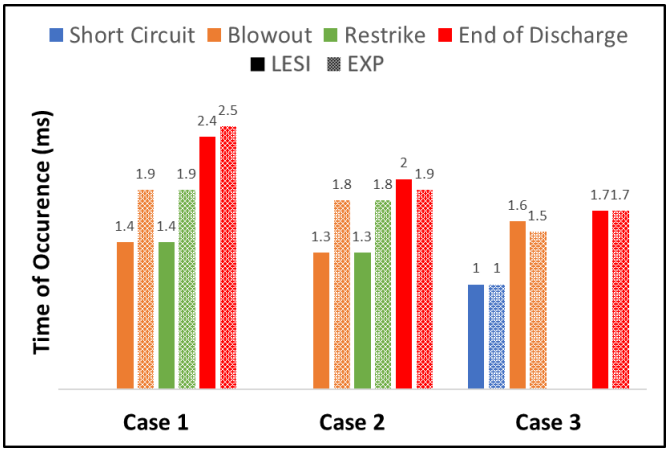

Figure 8: Summary of Table 2 in bar plot format. The solid bars represent results from the LESI simulations and the dashed bars refer to results from experiments.

The results shown in Figs. 2-8 highlight the LESI model's ability to predict the occurrence and sometimes the time of occurrence of spark channel shortening events (short-circuits, blowouts, and re-strikes). A summary of these predictions is shown in Table 2 and visualized in Fig. 8, where its parameters were matched against experimental data. These results are evidence that model performance is dependent on the accuracy of Eq. 1.

Reacting Ignition Simulations: Cases 4-9

Cases 4-9 simulate electrical discharge and ignition in a diluted reacting environment. Combustion was initiated as the ambient environment includes ethane and oxygen. As such, the spark channel length plot is replaced with a flame front location plot. Note that due to absence of data on the spark channel length for the reacting cases, no tuning of Eq. 1 was done against experimental electrical signals. Instead, the previously tuned parameters for Cases 1-3 and literature reported values were used as a starting point, before manually tuning to match the experimental voltage and power signals through a trial-and-error process.

Case 4

The ambient pressure in Case 4 is 15 bar and the fan speed is set to 5000 rpm, which is the reacting flow version of Case 1. The secondary circuit output from the simulation of Case 4 is shown in Fig. 9 (a), (b), and (c), compared to three experimental iterations of the same operating condition. Fig. 9 (d) shows the longitudinal flame front location compared to experiment. While the flame front growth is not entirely dependent on the ignition model and relies on other factors such as the grid size, combustion model, and velocity field, it is a good indicator of overall simulation accuracy including the ignition model.

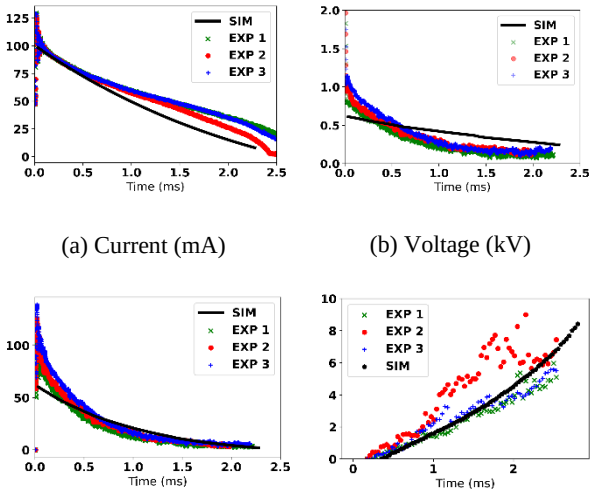

(a) Current (mA) (b) Voltage (kV)

(c) Power (W) (d) Flame Location (mm)

Figure 9: LESI model output for Case 4. The experiment numbers are different experimental iterations of the same operating condition.

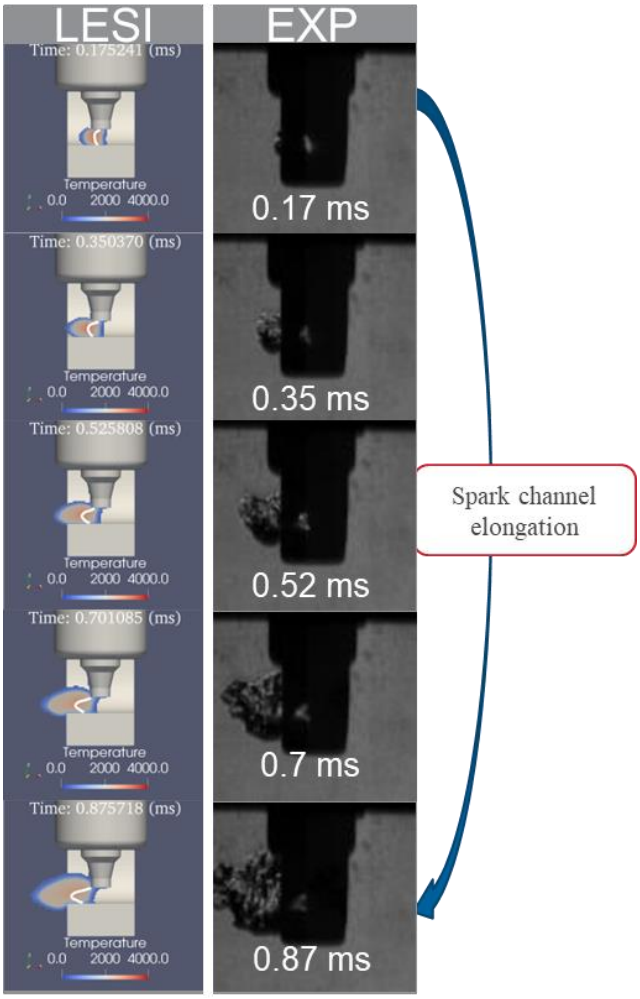

Figure 10: Spark channel elongation: simulation versus experiment for Case 4. No short-circuits or restrikes observed in experiments or predicted by the model.

Keeping in mind that for the reacting flow cases, the voltage expression was not tuned against experimental data, the inductive phase electrical current in Fig. 9 (a), starts at around 100 mA and decreases steadily until end of discharge around 2.4 ms. The current deviates from experimental results after 0.7 ms. The voltage and power in Figs. 9 (b) and (c) are underestimated at time earlier than 0.3 ms but show proper agreement with experimental results after that. The flame front location is well predicted as can be seen in Fig. 9 (d).

While previous operating conditions presented in this paper showed multiple spark-shortening events, Case 4 shows only spark elongation as shown in Fig. 10. Similarly, the LESI model reproduces this behavior where the simulation shows that no restrikes or short-circuits occur for this operating condition. The LESI model here predicts a correct shape of the spark channel while slightly overestimating its elongation, which is possibly due to inaccuracies in the flow field or channel initialization. Blowout and end of discharge are well predicted at around 2.3 ms.

Case 5

The ambient pressure in Case 5 is 15 bar and the fan speed is set to 10000 rpm. Like Fig. 8, Fig. 10 shows the electrical current, voltage, power, and flame front location compared to three experimental data sets.

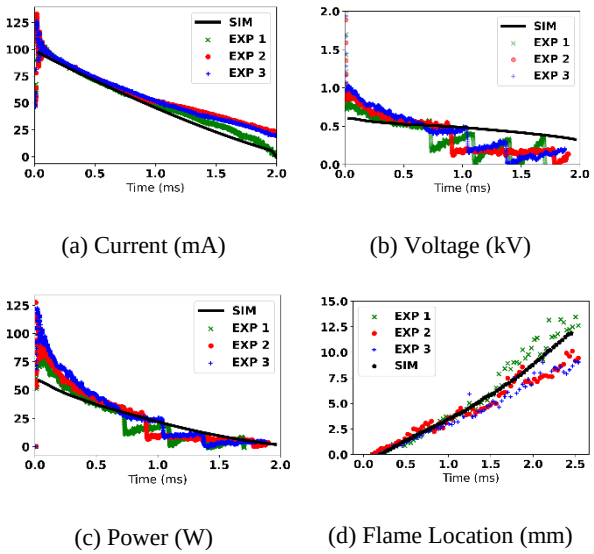

(a) Current (mA) (b) Voltage (kV)

(c) Power (W) (d) Flame Location (mm)

Figure 11: LESI model output for Case 5. The experiment numbers are different experimental iterations of the same operating condition.

The inductive phase electrical current in Fig. 11 (a), also starts at around 100 mA and decreases steadily until end of discharge around 2.0 ms. The current here shows better agreement with experimental data than Case 4. The voltage and power in Figs. 11 (b) and (c) are also underestimated at time earlier than 0.2 ms but show proper agreement with experimental results after that. This is possibly due to the breakdown voltage not being modeled as part of LESI. The flame front location is well predicted within the bounds of the experimental envelope as can be seen in Fig. 11 (d).

Like Case 4, Case 5 shows only spark channel elongation as can be seen in Fig. 12. The LESI model also reproduces this behavior where the simulation shows no occurrence of spark shortening events, which is expected for a relatively low pressure of 15 bar. The LESI model here predicts correct spark channel shape and elongation. In addition, blowout and end of discharge are well predicted at around 2.0 ms. In addition, LESI predicts more elongation for Case 5 compared to Case 4, which is expected when going from a 5000 to 10,000 rpm fan speed.

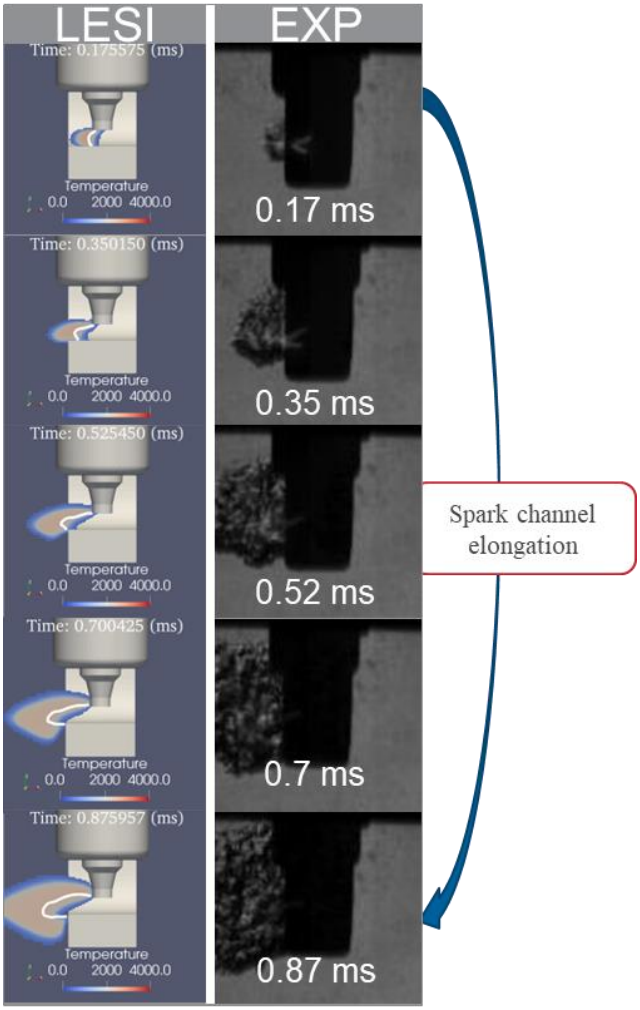

Figure 12:Spark channel elongation: simulation versus experiment for Case 5. No short-circuits or restrikes observed in experiments or predicted by the model.

Case 6

The ambient pressure in Case 6 is 30 bar and the fan speed is set to 5000 rpm. Like Figs. 9 and 11, Fig. 13 shows the electrical current, voltage, power, and flame front location compared to four experimental data sets.

Unlike the previous cases so far, the inductive phase electrical current in Fig. 13 (a), starts at around 90 mA and decreases steadily until end of discharge around 1.9 ms. The current here shows good agreement with experimental data at all times. Like other reacting flow cases so far, the voltage and power in Figs. 13 (b) and (c) are also underestimated at time earlier than 0.5 ms but show proper agreement with experimental results after that. The flame front location is well predicted at all times as can be seen in Fig. 13 (d).

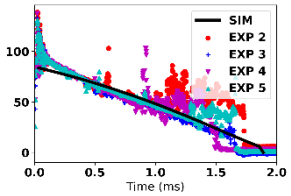

(a) Current (mA)

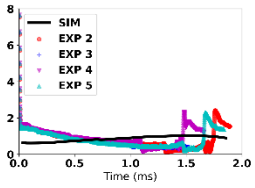

(b) Voltage (kV)

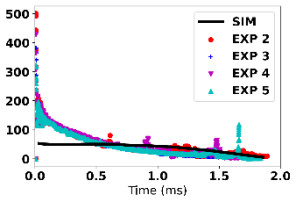

(c) Power (W)

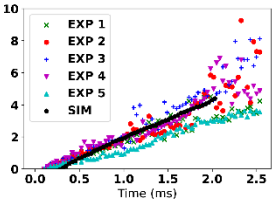

(d) Flame Location (mm)

Figure 13: LESI model output for Case 6. The experiment numbers are different experimental iterations of the same operating condition.

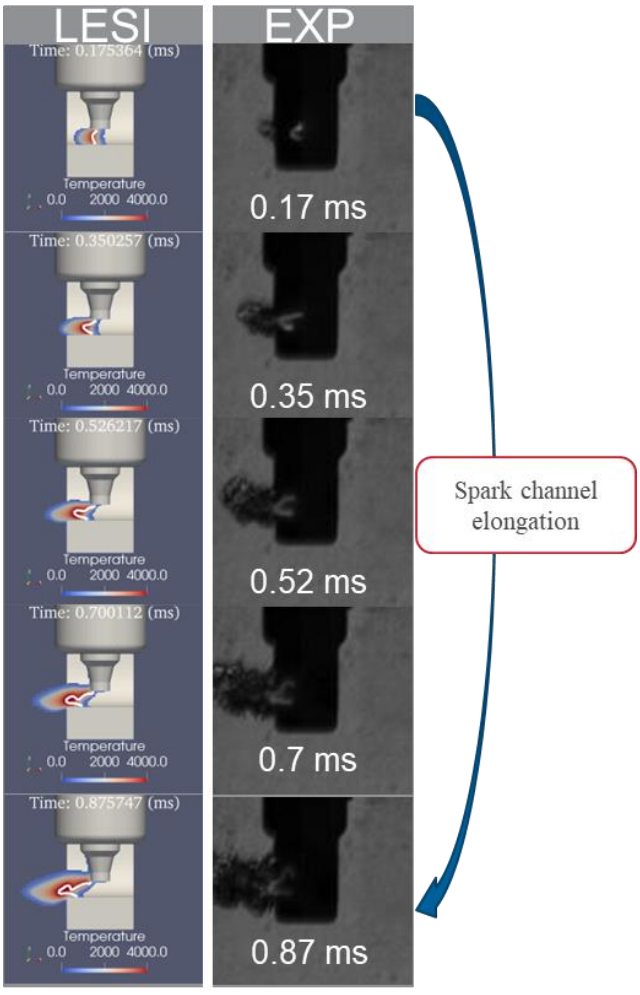

Figure 14: Spark channel elongation: simulation versus experiment Case 6. No short-circuits or restrikes observed in experiments or predicted by the model.

Similar to Cases 4 and 5, the spark channel elongates smoothly out of the spark gap with no short-circuits or significant spark channel folding. However, the arc exhibits an angular shape which is in line with experimental observations. For this case, this enhanced LESI model accurately predicts spark channel shape and elongation at all times, even if no short-circuiting or blowouts occur. Blowout and end of discharge are correctly predicted at around 1.9 ms.

Case 7

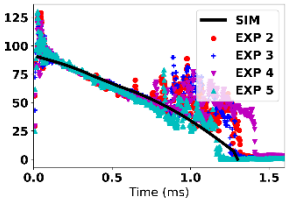

(a) Current (mA)

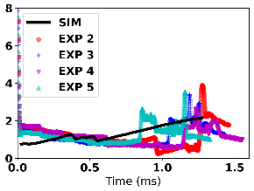

(b) Voltage (kV)

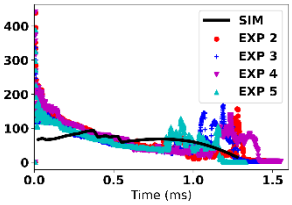

(c) Power (W)

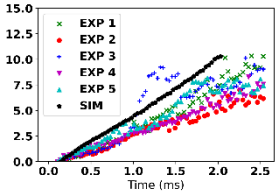

(d) Flame Location (mm)

Figure 15: LESI model output for Case 7. The experiment numbers are different experimental iterations of the same operating condition.

The ambient pressure in Case 7 is 30 bar and the fan speed is set to 10000 rpm. Like previous figures, Fig. 15 shows the electrical current, voltage, power, and flame front location compared to four experimental data sets.

Similar to Case 6, the inductive phase electrical current in Fig. 15 (a) starts at around 90 mA and decreases steadily until end of discharge around 1.3 ms. Here, the current shows good agreement with experimental data at all times and falls within the experimental envelope. The voltage and power in Figs. 15 (b) and (c) are also underestimated at times earlier than 0.25 ms but show proper agreement with experimental results after that. The flame front location is slightly overestimated as shown in Fig. 15 (d), which is likely due to combustion modeling and/or grid effects as the flame front location is in agreement with experimental data at times earlier than 0.4 ms.

As shown in Fig. 16, the arc at early times is similar in shape to the experiment. The LESI model correctly predicts the occurrence of one short-circuit, but at a later time (0.35-0.52 ms) than observed in experiment (0.17-0.35 ms). At 0.35 ms, the tip of the spark channel starts folding on itself and at 0.52 ms, the LESI model has short-circuited it to smooth out the spark channel shape. However, short circuiting is done just enough to avoid implausible folding while maintaining realistic spark channel elongation and overall shape without over-smoothing. The spark channel maintains accurate elongation throughout ignition with end of discharge occurring at around 1.3 ms in both simulation and experiment.

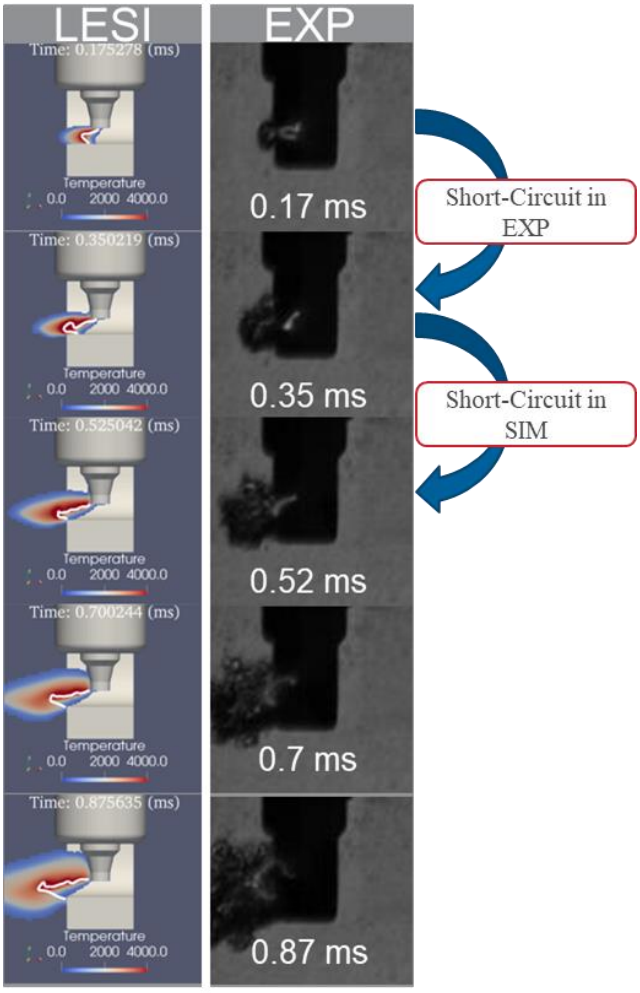

Figure 16: Spark channel elongation: simulation versus experiment for Case 7: Short-circuit observed in experiment between 0.17 and 0.35 ms. Short-circuit predicted by the model between 0.35 and 0.52 ms.

Case 8

The ambient pressure in Case 8 is 45 bar and the fan speed is set to 5000 rpm. Like previous figures, Fig. 17 shows the electrical current, voltage, power, and flame front location compared to five experimental data sets.

Unlike previous cases, here in Case 8, the inductive phase electrical current in Fig. 17 (a), starts at around 80 mA and decreases steadily until end of discharge around 0.8 ms. The current is overestimated between 0.1 and 0.6 ms. On the other hand, the voltage and power in Figs. 17 (b) and (c) are well predicted at all times and fall within the experimental envelope. The flame front location matches experiment as shown in Fig. 17 (d).

Figure 18 shows the spark channel elongation for Case 8. Despite a retarded lower end point movement, the spark channel maintains good agreement with the experiments in terms of shape and elongation. A short-circuit is observed in the experiment and predicted by the model between 0.52 ms and 0.7 ms. Finally, the discharge ends with a blowout event at around 0.8 ms.

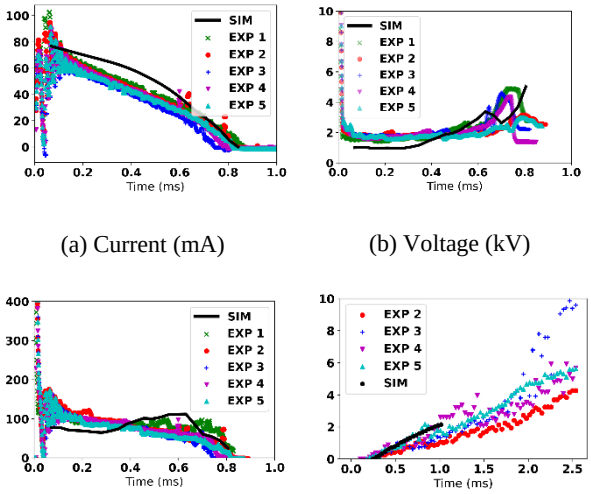

Figure 17: LESI model output for Case 8. The experiment numbers are different experimental iterations of the same operating condition.

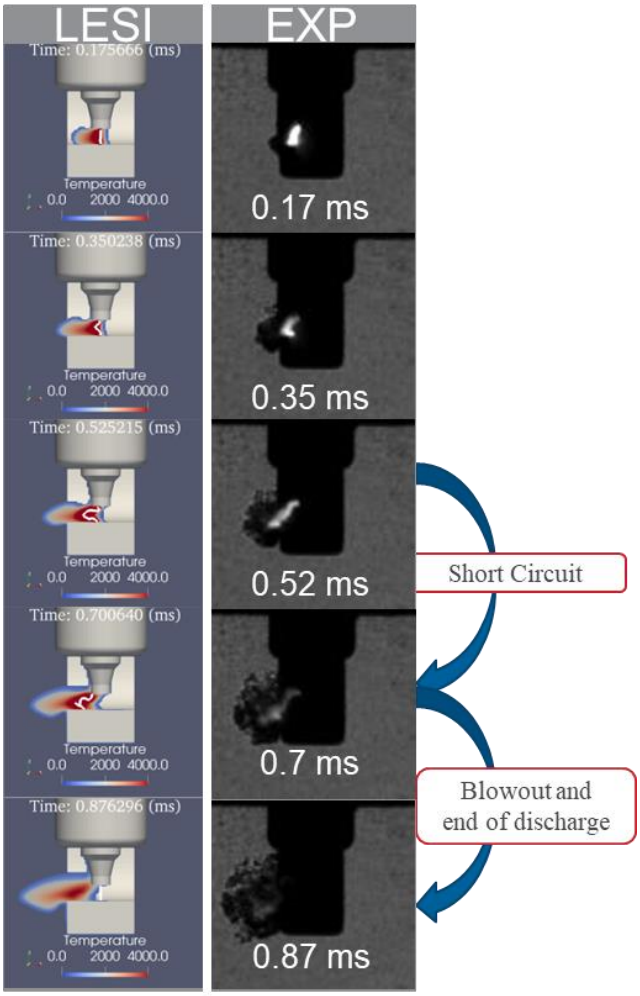

Figure 18: Spark channel elongation: simulation versus experiment for Case 8: Short-circuit observed in experiment and predicted by LESI between 0.52 and 0.7 ms. Blowout/end of discharge correctly predicted between 0.7 and 0.87 ms

Case 9

The ambient pressure in Case 9 is 45 bar and the fan speed is set to 10000 rpm. Like previous cases, Fig. 19 shows the electrical current, voltage, power, and flame front location compared to two experimental data sets.

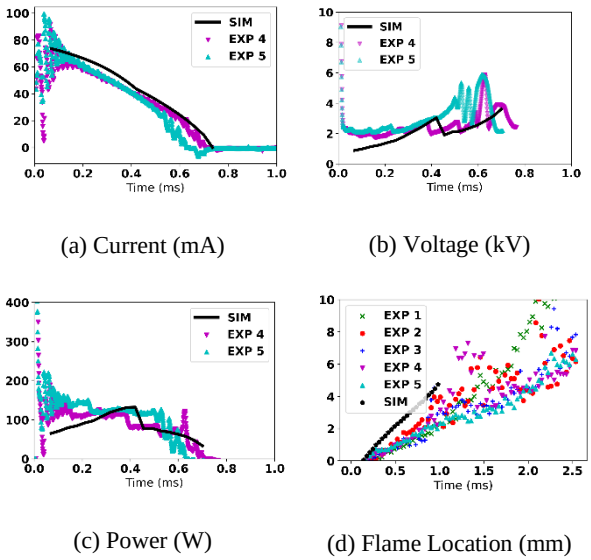

(a) Current (mA) (b) Voltage (kV)

(c) Power (W) (d) Flame Location (mm)

Figure 19: LESI model output for Case 9. The experiment numbers are different experimental iterations of the same operating condition.

Similar to Case 8, the inductive phase electrical current in Fig. 19 (a), starts at around 80 mA and decreases steadily until end of discharge around 0.7 ms. The current is overestimated between 0.1 and 0.4 ms. On the other hand, the voltage and power in Figs. 19 (b) and (c) are well predicted at all times and fall within the experimental envelope. The flame front location is overestimated here as shown in Fig. 19 (d), which, similar to Case 7, could be related grid-related, combustion, or flow field errors.

In a similar manner to all previous cases, Fig. 20 shows the spark channel elongation for Case 9 compared to experimental Schlieren images. Similar to Case 8, a retarded lower end point movement is observed. However, despite this fact, the spark channel maintains good agreement with the experiments in terms of shape and elongation. The model replicates the shape of the arc quite well at 0.35 ms with a “folded and angular” leading edge, which then short circuits between 0.35 ms and 0.52 ms in both simulation and experiment. Finally, blowout occurs at around 0.7 ms, in both simulation and experiment.

The results shown in Figs. 9-20 emphasize that the LESI model with the additional sub-models can maintain and predict the spark channel elongation while handling the on-line secondary circuit, short-circuit, and blowout/restrike sub-models to simulate spark shortening events. A summary of these predictions for Cases 4-9 (dilute reacting flow) is shown in Table 3 and visualized in Fig. 21. While for these cases Eq. 1 was not tuned against experimental data, the model was still able to predict the overall discharge behavior, spark channel elongation, the occurrence of shortening events, and end of discharge.

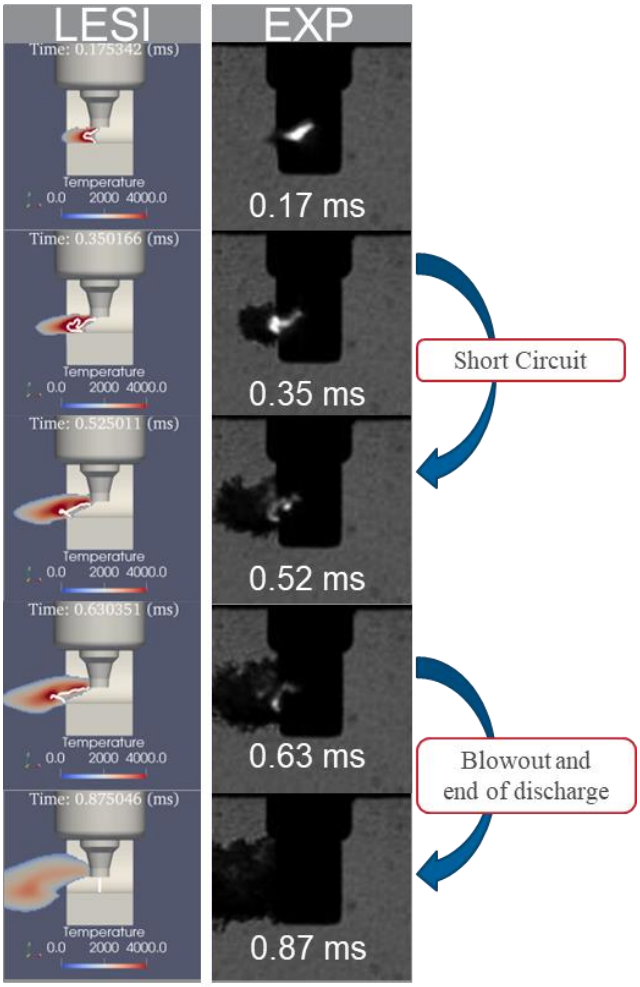

Figure 20: Spark channel elongation: simulation versus experiment for Case 9: Short-circuit observed in experiment and predicted by LESI between 0.35 and 0.52 ms. Blowout/end of discharge correctly predicted between 0.7 and 0.87 ms

Table 3: Short-circuit and end of discharge time of occurrence predictions made by the LESI model, compared to experiment for cases 4-9. No restrike was observed in experiments or simulations for these cases.

Case	Short Circuit (ms)	End of Discharge (ms)
4 – SIM	-	2.3
4 – EXP	-	2.4
5 – SIM	-	2.0
5 – EXP	-	2.0
6 – SIM	-	1.9
6 – EXP	-	1.8
7 – SIM	0.52	1.3
7 – EXP	0.35	1.3
8 – SIM	0.7	0.8
8 – EXP	0.7	0.8
9 – SIM	0.52	0.7
9 – EXP	0.52	0.7

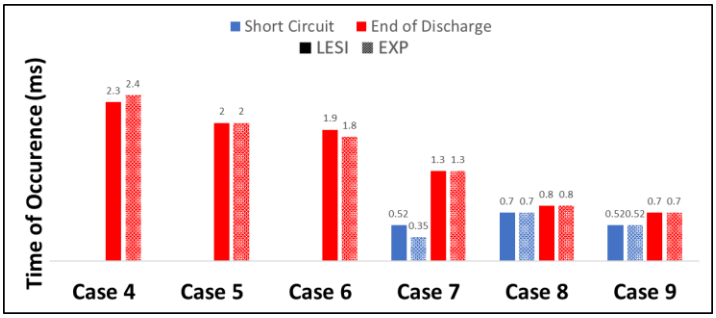

Figure 21: Summary of Table 3 in bar plot format. The solid bars represent results from the LESI simulations and the dashed bars refer to results from experiments.

Conclusions and Next Steps

In this paper, a hybrid Langrangian-Eulerian Spark-Ignition (LESI) model with additional spark shortening capabilities [36] was used in a constant volume combustion vessel to simulate electrical discharge in three inert flow operating conditions and ignition in six dilute reacting flow operating conditions. The LESI model enhanced with the added sub-models accurately predicted and reproduced the following parameters:

1. the secondary circuit output including the voltage, current, and power
2. the spark channel elongation and arc shape
3. the occurrence of spark shortening events such as short-circuits, restrikes, and blowouts
4. the end of electrical discharge

The added sub-models were able to maintain a realistic arc shape despite excessive folding in certain conditions. Qualitatively, the arc retained its angular characteristics, which were observed in experiment, while spark shortening events were triggered were necessary. It is important to note that the most important parameter in the model is the secondary circuit voltage empirical expression. The coefficients of this empirical expression are vital for the overall accuracy of the model.

Possible future additions to the LESI model include:

1. improvements to the spark channel voltage expression to include spark channel length dependence
2. improvements to the spark channel initialization schemes to account for the stochasticity observed in experiment.

References

1. U. S. E. I. A. (EIA), ANNUAL ENERGY OUTLOOK, 2021. URL https://www.eia.gov/outlooks/aeo/
2. K. Ikeya, M. Takazawa, T. Yamada, S. Park, et al., “Thermal Efficiency Enhancement of a Gasoline Engine”, SAE International Journal of Engines 8 (4):1579-1586, 2015, doi:10.4271/2015-01-1263.
3. K. Nakata, S. Nogawa, D. Takahashi, Y. Yoshihara, et al., “Engine Technologies for Achieving 45% Thermal Efficiency of S.I. Engine”, SAE Technical Paper 2015-01-1896, 2015, doi:10.4271/2015-01-1896.
4. S. Pischinger and J. B. Heywood, “How Heat Losses to the Spark Plug Electrodes Affect Flame Kernel Development in an SI-Engine”, SAE Technical Paper 900021, 1995, doi:10.4271/900021.
5. B. Johansson, “Cycle to Cycle Variations in S.I. Engines - The Effects of Fluid Flow and Gas Composition in the Vicinity of the Spark Plug on Early Combustion”, SAE Technical Paper 962084, 1996, doi:10.4271/962084.
6. C. R. Stone, A. G. Brown, and P. Beckwith, “Cycle-by-Cycle Variations in Spark Ignition Engine Combustion - Part II: Modelling of Flame Kernel Displacements as a Cause of Cycle-by-Cycle Variations”, SAE Technical Paper 960613, 1996, doi:10.4271/960613.
7. F. A. Ayala and J. B. Heywood, “Lean SI Engines: The role of combustion variability in defining lean limits”, SAE Technical Paper 2007-24-0030, 2007, doi:10.4271/2007-24-0030.
8. S. J. Kazmouz, D. C. Haworth, P. Lillo, and V. Sick, “Large-eddy simulations of a stratifed-charge direct-injection spark-ignition engine: Comparison with experiment and analysis of cycle-to-cycle variations”, Proceedings of the Combustion Institute 38 (4):5849-5857, 2021, doi:10.1016/j.proci.2020.08.035.
9. T. Alger, J. Gingrich, C. Roberts, B. Mangold, et al., “A High-Energy Continuous Discharge Ignition System for Dilute Engine Applications”, SAE Technical Paper 2013-01-1628, 2013, doi:10.4271/2013-01-1628.
10. M. Thiele, S. Selle, U. Riedel, J. Warnatz, et al., “Numerical simulation of spark ignition including ionization”, Proceedings of the Combustion Institute 28 (1):1177-1185, 2000, doi:10.1016/S0082-0784(00)80328-8.
11. X. Yang, A. Solomon, and T.-W. Kuo, “Ignition and Combustion Simulations of Spray-Guided SIDI Engine using Arrhenius Combustion with Spark-Energy Deposition Model”, SAE Technical Paper 2012-01-0147, 2012, doi:10.4271/2012-01-0147.
12. O. Colin and K. Truffin, “A spark ignition model for large eddy simulation based on an FSD transport equation (ISSIM-LES)”, Proceedings of the Combustion Institute 33 (2): 3097-3104, 2011, doi:10.1016/j.proci.2010.07.023.
13. G. Lacaze, E. Richardson, and T. Poinsot, “Large eddy simulation of spark ignition in a turbulent methane jet”, Combustion and Flame 156 (10): 1993-2009, 2009, doi:10.1016/j.combustflame.2009.05.006.
14. Q. Malé, G. Staffelbach, O. Vermorel, A. Misdariis, et al., “Large eddy simulation of pre-chamber ignition in an internal combustion engine”, Flow Turbulence and Combustion 103:465-483, 2019, doi:10.1007/s10494-019-00026-y
15. S. J. Kazmouz, R. Scarcelli, M. Bresler, E. Blash, et al., “Modeling Spark Channel Elongation at Different Flow Magnitudes and Pressure Conditions”, presented at 12th U. S. National Combustion Meeting, USA, May 24-26, 2021.
16. S. D. Givler, M. Raju, E. Pomraning, P. K. Senecal, et al., “Gasoline Combustion Modeling of Direct and Port-Fuel Injected Engines using a Reduced Chemical Mechanism”, SAE Technical Paper 2013-01-1098, 2013, doi:10.4271/2013-01-1098.
17. C. Iacovano, Y. Zeng, M. Anbarasu, S. Fontanesi, et al., “Validation of a LES Spark-Ignition Model (GLIM) for Highly-Diluted Mixtures in a Closed Volume Combustion Vessel”, SAE Technical Paper 2021-01-0399, 2021, doi:10.4271/2021-01-0399.
18. Z. Tan and R. D. Reitz, “An ignition and combustion model based on the level-set method for spark ignition engine multidimensional modeling”, Combustion and Flame 145 (1):1-15, 2006, doi:10.1016/j.combustflame.2005.12.007.
19. J.-M. Duclos and O. Colin, (2-25) “Arc and Kernel Tracking Ignition Model for 3D Spark-Ignition engine calculations((SI-7)

S. I. Engine Combustion 7-Modeling)", The Proceedings of the International symposium on diagnostics and modeling of combustion in internal combustion engines 01.204:46, 2001, doi:10.1299/jmsesdm.01.204.46.
20. R. Dahms, T. Fansler, M. Drake, T.-W. Kuo, et al., "Modeling ignition phenomena in spray-guided spark-ignited engines", Proceedings of the Combustion Institute 32 (2):2743-2750, 2009, doi:10.1016/j.proci.2008.05.052.
21. L. Fan, G. Li, Z. Han, and R. D. Reitz, "Modeling Fuel Preparation and Stratified Combustion in a Gasoline Direct Injection Engine", SAE Technical Paper 1999-03-0175, 1999, doi:10.4271/1999-01-0175.
22. Sforza, L., Lucchini, T., Montenegro, G., Aksu, C. et al., "Modeling the Effects of the Ignition System on the CCV of Ultra-Lean SI Engines using a CFD RANS Approach," SAE Technical Paper 2021-01-1147, 2021, doi:10.4271/2021-01-1147.
23. Sforza, L., Lucchini, T., and D'Errico, G., "3D-CFD Methodologies for a Fast and Reliable Design of Ultra-Lean SI Engines," SAE Technical Paper 2022-37-0006, 2022, doi:10.4271/2022-37-0006.
24. O. Colin, M. Ritter, C. Lacour, K. Truffin, et al. "Dns and les of spark ignition with an automotive coil", Proceedings of the Combustion Institute 37 (4)"4875-4883, 2019, doi:10.1016/j.proci.2018.08.021.
25. S. J. Kazmouz, R. Scarcelli, J. Kim, Z. Cheng, et al., "High-Fidelity Energy Deposition Ignition Model coupled with Flame Propagation Models at Engine-like Flow Conditions", Journal of Engineering for Gas Turbines and Power, doi:10.1115/1.4056098
26. T. Shiraishi, A. Teraji, and Y. Moriyoshi, "The Effects of Ignition Environment and Discharge Waveform Characteristics on Spark Channel Formation and Relationship between the Discharge Parameters and the EGR Combustion Limit", SAE Technical Paper 2015-01-1895, 2015, doi:10.4271/ 2015-01-1895.
27. N. Hayashi, A. Sugiura, Y. Abe, and K. Suzuki, "Development of Ignition Technology for Dilute Combustion Engines", SAE Technical Paper 2017-01-0676, 2017, doi:10.4271/2017-01-0676.
28. S. Sayama, M. Kinoshita, Y. Mandokoro, and T. Fuyuto, "Spark ignition and early flame development of lean mixtures under high-velocity flow conditions: An experimental study", International Journal of Engine Research 20 (2):236-246, 2019, doi:10.1177/1468087417748517
29. T. Lucchini, L. Cornolti, G. Montenegro, G. D'Errico, et al., "A Comprehensive Model to Predict the Initial Stage of Combustion in SI Engines", SAE Technical Paper 2013-01-1087, 2013, doi:10.4271/2013-01-1087.
30. T. Hori, "Modeling of spark channel elongation and restrike in si engine", Transactions of Society of Automotive Engineers of Japan 48 (3):641-647, 2017, doi:10.11351/jsaeronbun.48.641
31. H. Ge and P. Zhao, "A Comprehensive Ignition System Model for Spark Ignition Engines", presented at ASME Internal Combustion Engine Division Fall Technical Conference, USA, November 4-7, 2018, doi:10.1115/ICEF2018-9574.
32. R. Masuda, S. Sayama, T. Fuyuto, M. Nagaoka, et al., "Application of Models of Short Circuits and Blow-Outs of Spark Channels under High-Velocity Flow Conditions to Spark Ignition Simulation", SAE Technical Paper 2018-01-1727, 2018, doi:10.4271/2018-01-1727.
33. S. Sayama, M. Kinoshita, Y. Mandokoro, R. Masuda, et al., "Quantitative Optical Analysis and Modelling of Short Circuits and Blow-Outs of Spark Channels under High-Velocity Flow Conditions", SAE Technical Paper 2018-01-1728, 2018, doi:10.4271/2018-01-1728.
34. J. Kim and R. W. Anderson, "Spark Anemometry of Bulk Gas Velocity at the Plug Gap of a Firing Engine", SAE Technical Paper 952459, 1995, doi:10.4271/952459.
35. R. Maly, H. Meinel, and E. Wagner, "Novel Method for Determining General Flow Parameters from Conventional Spark Discharge", Vol. 67, IMechE Conf. Trans. C.:27-32, 1985
36. S. Kazmouz, R. Scarcelli, M. Bresler, E. Blash, et al., "A Comprehensive Model to Capture Electrical Discharge and Spark Channel Evolution during Spark-Ignition Processes", Combustion and Flame 248: 112589, 2022, doi:10.1016/j.combustflame.2022.112589
37. R. Scarcelli, A. Zhang, T. Wallner, S. Som, et al., "Development of a Hybrid Lagrangian-Eulerian Model to Describe Spark-Ignition Processes at Engine-Like Turbulent Flow Conditions", Journal of Engineering for Gas Turbines and Power 141 (9):091009, 2019, doi:10.1115/1.4043397.
38. Kazmouz, S. J., Scarcelli, R., Cheng, Z., Dai, M., Pomraning, E., Senecal, P. K., & Sjöberg, M. (2022). Coupling a lagrangian–eulerian spark-ignition (LESI) model with Les combustion models for engine simulations. Science and Technology for Energy Transition, 77, 10. doi:10.2516/stet/2022009
39. A. Zhang, R. Scarcelli, S.-Y. Lee, T. Wallner, et al., "Numerical Investigation of Spark Ignition Events in Lean and Dilute Methane/Air Mixtures Using a Detailed Energy Deposition Model", SAE Technical Paper 2016-01-0609, 2016, doi:10.4271/2016-01-0609.
40. K. J. Richards, P. K. Senecal, and E. Pomraning, CONVERGE 3.0, CONVERGENT SCIENCE, Madison, WI, 2021.

Contact Information

Samuel J. Kazmouz – skazmouz@anl.gov – (630) 252-3740

Acknowledgments

The submitted manuscript has been created by UChicago Argonne, LLC, Operator of Argonne National Laboratory ("Argonne") **and by FCA US LLC.** Argonne, a U.S. Department of Energy Office of Science laboratory, is operated under Contract No. DE-AC02-06CH11357.

The U.S. Government retains for itself, and others acting on its behalf, a paid-up nonexclusive, irrevocable worldwide license in said article to reproduce, prepare derivative works, distribute copies to the public, and perform publicly and display publicly, by or on behalf of the Government.

This research is funded by DOE's Vehicle Technologies Program, Office of Energy Efficiency and Renewable Energy, under the FY19 Technology Commercialization Fund (TCF) program. The authors would like to express their gratitude to Gurpreet Singh and Mike Weismiller, program managers at DOE, for their support.

Numerical simulations were run on the Blues and Bebop Clusters at the LCRC, Argonne National Laboratory.

DISCLAIMERS: Neither the United States Government nor any agency thereof, nor UChicago Argonne, LLC, nor FCA US LLC, nor any of their employees or officers, makes any warranty, express or implied, or assumes any legal liability or responsibility

for the accuracy, completeness, or usefulness of any information, apparatus, product, or process disclosed, or represents that its use would not infringe privately owned rights. Reference herein to any specific commercial product, process, or service by trade name, trademark, manufacturer, or otherwise, does not necessarily constitute or imply its endorsement, recommendation, or favoring by the United States Government or any agency thereof. The views and opinions of document authors expressed herein do not necessarily state or reflect those of the United States Government or any agency thereof, Argonne National Laboratory, UChicago Argonne, LLC, or FCA US LLC.

Definitions/Abbreviations

AKTIM	Arc and kernel tracking ignition model
CFD	Computational Fluid Dynamics
DPIK	Discrete particle ignition kernel
GLIM	GruMo-UniMORE LES ignition model
ICE	Internal combustion engine
IMEP	Indicated mean effective pressure
ISSIM	Imposed stretch spark ignition model
LDV	Light-duty vehicle
LESI	Lagrangian-Eulerian spark-ignition
OEM	Original equipment manufacturer
SI	Spark-ignition
SparkCIMM	Spark channel ignition monitoring model
UDF	User-defined function